

# Growth, overprinting, and stabilization of Proterozoic Provinces in the southern Lake Superior region

Daniel Holm<sup>a,\*</sup>, L. Gordon Medaris, Jr.<sup>b</sup>, Kalin T. McDannell<sup>c</sup>, David A. Schneider<sup>d</sup>, Klaus Schulz<sup>e</sup>, Bradley S. Singer<sup>b</sup>, Brian R. Jicha<sup>b</sup>

<sup>a</sup>*Dept. of Geology, Kent State University, Kent, OH*

<sup>b</sup>*Dept. of Geoscience, UW-Madison, WI*

<sup>c</sup>*Geological Survey of Canada, Calgary, AB*

<sup>d</sup>*Dept. of Earth Science, University of Ottawa, Ottawa, ON*

<sup>e</sup>*U.S. Geological Survey, Reston, VA*

## **Abstract**

New geochronologic data in the southern Lake Superior region provide key information on the timing and nature of tectonic activity that pre-and post-date initial Paleoproterozoic growth of Laurentia during the geon 18 Penokean orogeny. The obducted Pembine ophiolite formed along the edge of a Paleoproterozoic ocean basin at least 30 m.y. prior to Penokean island arc/microcontinent accretion beginning at 1860 Ma. Following Penokean orogenesis, intrusion of mafic dikes at  $1817 \pm 2$  Ma indicate a period of extension that coincided with a 30 m.y. gap in orogenic felsic magmatism at 1835-1805 Ma (between the Penokean and Yavapai orogenies) and likely represents relaxation of Penokean compression and a tectonic switch to intra-arc extension related to initiation of Yavapai subduction. Subsequent Yavapai arc accretion (1750-1720 Ma) resulted in pervasive ductile deformation of the dikes and host rocks at temperatures of  $\sim 700$  °C, previously attributed to Penokean deformation. Geon 16 Mazatzal overprinting of the accreted Penokean and Yavapai provinces was widespread but of overall lower metamorphic grade (greenschist facies), and the thermal effects of the 1476-1470 Ma shallow level Wolf River batholith was limited to a 10-15 km wide contact zone surrounding the intrusion.

In contrast to the Archean Superior Province to the north, Paleoproterozoic terranes in the southern Lake Superior area experienced widespread low-temperature reheating and cooling of shallow crustal levels at ca. 1.1-1.0 Ga attributed primarily to magmatic underplating with little subsequent Neoproterozoic exhumation. In the southern Lake Superior region widespread magmatic underplating likely thickened, strengthened, and stabilized Proterozoic Penokean-Mazatzal lithosphere but destabilized Archean cratonized Superior Province lithosphere to the north.

\* Corresponding author: Dept of Geology, 325 S. Lincoln Street, Kent State University, Kent, OH 44242, USA. dholm@kent.edu.

*Keywords:* geochronology, mafic magmatism, Proterozoic tectonics, stabilization, Penokean, Yavapai, thermochronology

## **1. Introduction**

Proterozoic continental growth following assembly of the Laurentian core is conventionally attributed to successive accretion of numerous juvenile arcs along the margins of the Archean Superior and Wyoming provinces (Karlstrom et al., 2001). Late Paleoproterozoic (1900-1600 Ma) juvenile arc rocks in the upper Great Lakes region formed during three separate accretionary tectonic episodes as the North American craton grew southward (Fig. 1; NICE Working Group, 2007).

The oldest of these accretionary orogens, the 1875-1835 Ma Penokean province (Van Schmus, 1980), is located in the southern Lake Superior region (Wisconsin, northern Michigan, east-central Minnesota, and southwestern Ontario). The Penokean province includes many of the

hallmarks of accretion, including an ophiolite-island arc complex, the Pembine ophiolite, that was obducted along the Niagara fault, a Paleoproterozoic suture zone (Schulz and Cannon, 2007)

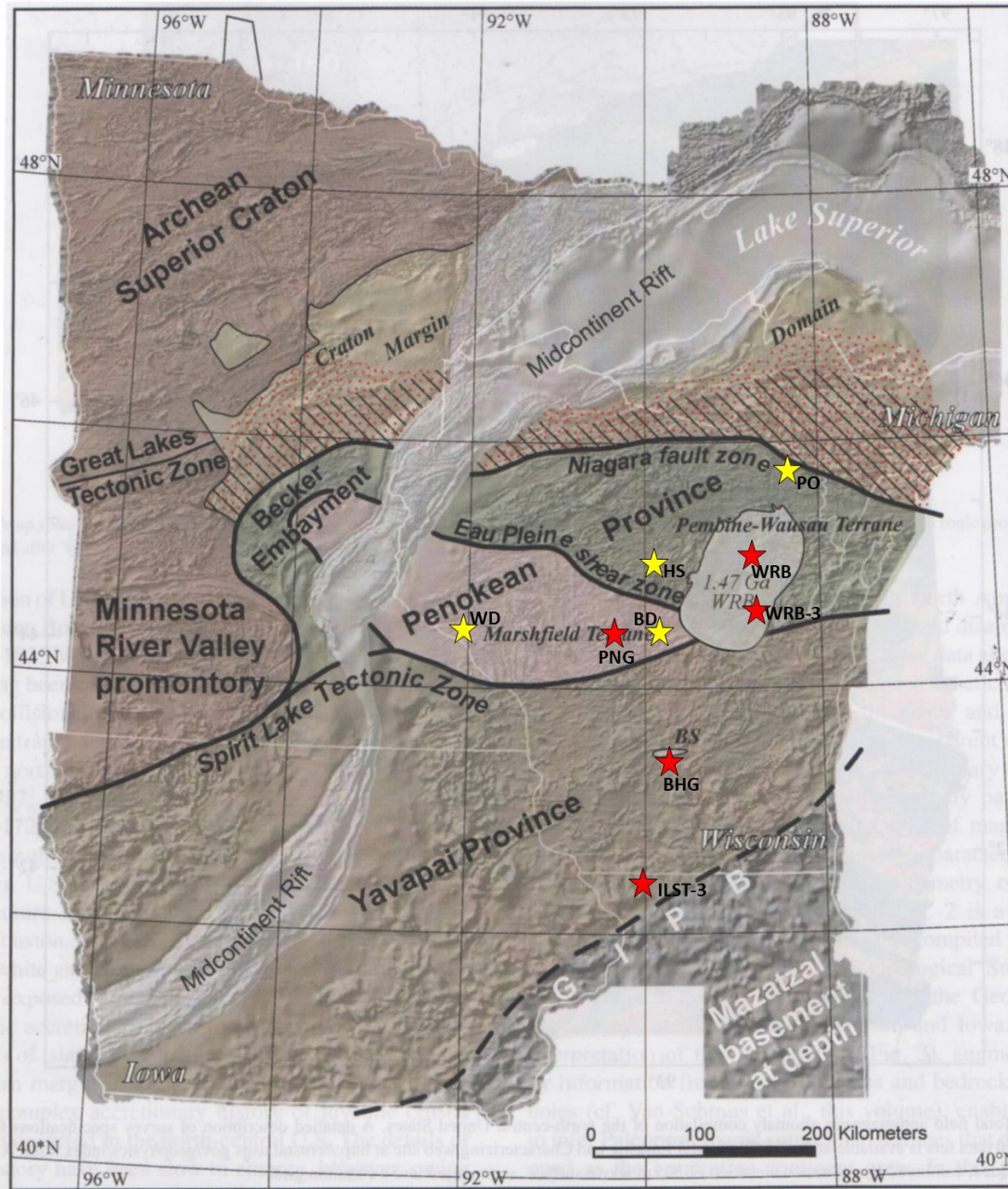


Fig. 1: Geologic terrane map of Precambrian basement rocks in the northern U.S. continental interior (after NICE Working Group, 2007). Yellow stars represent localities with higher temperature age data discussed in the text (BD: Biron dam; HS: Hamburg schist; PO; Pembine ophiolite; WD: Wissota dam). Red stars represent localities with low-T feldspar Ar/Ar ages (PNG: geon 18 Neillville granite; BHG: geon 17 Baxter Hollow granite; ILST-3: geon 14 granite core; WRB and WRB-3: geon 14 Wolf River granite).

The Penokean terrane was variably overprinted by magmatic, tectonic, and thermal episodes associated with pulses of geon 17 (Yavapai), geon 16 (Mazatzal), geon 14 (Wolf River batholith) and geon 11 (Mid-Continent Rift) tectonomagmatic events. Determining the timing, nature and relative contribution of these subsequent events is critical for properly ascribing structures, strain features, and degree of metamorphism/reheating to their correct tectonomagmatic event (Craddock et al., 2018). In this paper, we present geochronologic data that provide key information on the timing, extent, and nature of tectonic activity that bounds and overprints the Penokean orogeny.

The Pembine ophiolite formed at least 30 m.y. prior to initial accretion of the Penokean island arc with the southern margin of the Superior craton at 1860 Ma. Following Penokean orogenesis, a temporary switch to tectonic extension occurred at 1817 Ma during a 30 m.y. hiatus between the end of Penokean magmatism at 1835 Ma and the start of Yavapai magmatism at 1805 Ma. Additionally, geothermometry and thermochronologic data enable us to document strong penetrative geon 17 (Yavapai) ductile deformation and metamorphism of the southern Penokean orogen north of the Spirit Lake tectonic zone and more limited metamorphic overprinting associated with geon 16 Mazatzal accretion and subsequent emplacement of the geon 14 Wolf River batholith. Finally, low temperature geon 11-10 cooling occurred subsequent to widespread reheating related to geon 11 mantle plume heating and magmatic underplating that ultimately strengthened and stabilized the amalgamated Proterozoic continental lithosphere, while destabilizing Archean lithosphere to the north.

## **2. Tectonic setting of the southern Lake Superior region**

In the southern Lake Superior region, the 1875-1835 Ma Penokean orogeny represents an island-arc/microcontinent collision that deformed and metamorphosed Archean basement and ca. 2100 Ma continental passive margin rocks (Schulz and Cannon, 2007; Fig. 1), some of which may be as young as ca. 1900 Ma (Pietrzak-Renaud and Davis, 2014). In northern Wisconsin, the steep, south-dipping Niagara fault zone (NFZ) is interpreted to be an 1860 Ma suture that separates deformed continental margin rocks on the north from tholeiitic and calc-alkalic volcanic and plutonic arc rocks of the Wisconsin magmatic terranes (WMT) to the south. The WMT consists of a northern primitive oceanic to evolved island arc-complex, the Pembine-Wausau terrane, that is separated from a southern exotic Archean microcontinent, the Marshfield terrane, by the steeply south-dipping Eau Pleine shear zone (EPSZ), also interpreted as a paleo-suture. Penokean volcanic and plutonic rocks (Sims et al., 1989; Van Wyck, 1995), which overlie and intruded the Archean gneisses of the Marshfield terrane, are deformed into steeply plunging folds with associated steep stretching lineations. The strong ductile deformation and coeval metamorphism of the Penokean igneous rocks has been historically attributed solely to Penokean orogenic deformation (Myers et al., 1980; Maass et al., 1980; Maass, 1983). Undeformed granites emplaced between 1836 and 1834 Ma (Sims et al., 1989; Schneider et al., 2002) pierce the Niagara and the Eau Pleine sutures and mark the upper bound on the timing of Penokean orogenesis (Schulz and Cannon, 2007).

Following a 30 m.y. hiatus in magmatism after Penokean orogenesis, renewed felsic plutonism beginning at 1805 Ma (Humboldt granite, northern MI) heralded the onset of abundant long-lived (50 m.y.) magmatism that generally migrated southeastward across the accreted Penokean crust and may be related to a slab window or slab breakoff event associated with northwest-directed subduction of Yavapai oceanic lithosphere beneath the newly accreted

Penokean terrane (Holm et al., 2005). In central Wisconsin (Fig. 1), aeromagnetic data indicate that the Penokean Marshfield and Pembine-Wausau terranes and the Eau Pleine shear zone are truncated by the east-northeast trending Spirit Lake tectonic zone (SLTZ), interpreted to be a northerly dipping Yavapai-age suture (NICE Working Group, 2007; Chichester et al., 2018). Yavapai arc accretion along the SLTZ likely occurred between 1750 and 1700 Ma, prior to deposition of Baraboo Interval supermature quartzites, which blanketed both the Penokean and Yavapai terranes (Dott, 1983; Holm et al., 1998b; Medaris et al., 2003; Schwartz et al., 2018; Stewart et al., 2018).

Archean gneisses and Paleoproterozoic continental margin rocks north and west of the NFZ underwent two episodes of medium pressure amphibolite-facies metamorphism; first during tectonic burial associated with Penokean accretion and second, associated with Yavapai magmatism (primarily east-central Minnesota, Holm et al., 1998a) and coeval gneiss dome formation during collapse and exhumation of the overthickened Penokean orogenic crust (primarily northern Michigan; Schneider et al., 2004). South of the NFZ throughout the Pembine-Wausau terrane in Wisconsin, metamorphism varies from upper greenschist to middle amphibolite facies (Geiger and Guidotti, 1989).

The geon 17 Yavapai tectonomagmatic event was followed by late geon 16 Mazatzal terrane accretion (Karlstrom and Bowring, 1993; Karlstrom et al., 2001), which (re)metamorphosed much of the previously accreted Penokean and Yavapai arc terranes (Dott, 1983; Holm et al., 1998b, 2007). In northwestern Wisconsin, Holm et al. (1998b) inferred the existence of a Mazatzal-age tectonic front, marked by the northern limit of folded quartzite spatially coinciding with reset ( $<1620$  Ma)  $^{40}\text{Ar}/^{39}\text{Ar}$  mica ages in basement rocks, which interestingly, also roughly coincides with the trace of the NFZ. Mazatzal-age metamorphism in much of Wisconsin is largely greenschist facies, having reached regional amphibolite facies only further

south in crust more proximal to the Mazatzal/Yavapai tectonic boundary (NICE Working Group, 2007; Van Schmus et al., 2007). New detrital zircon ages from the folded Waterloo quartzite and Baldwin conglomerate in Wisconsin establish post-Mazatzal deposition for some of the Proterozoic quartzites, and  $^{40}\text{Ar}/^{39}\text{Ar}$  ages for axial-planar muscovite in the Seeley Slate, Baraboo Quartzite, and Waterloo Quartzite indicate subsequent deformation during the ca. 1470–1460 Ma Wolf River tectonomagmatic event (Medaris et al., 2018, 2019; Schwartz et al., 2018).

South of the SLTZ, the geophysical character of the crust throughout southern Wisconsin indicates that much of the Mazatzal and Yavapai arc terranes were intruded by the ca. 1475–1430 Ma granites of the Eastern Granite Rhyolite Province, part of an extensive suite of magmatism that transects much of the southern part of the North American continent (Anderson, 1983). One of the oldest and largest intrusive bodies of this suite, the 1470–1476 Ma Wolf River batholith (Dewane and Van Schmus, 2007) and associated plutons in central Wisconsin, intruded juvenile rocks of the Penokean province mostly north of the Spirit Lake tectonic zone (Fig. 1).  $^{40}\text{Ar}/^{39}\text{Ar}$  plateau ages of 1450–1470 Ma from fine-grained muscovite in Baraboo Interval quartzites reflect widespread, but stratigraphically localized, hydrothermal activity and potassic metasomatism related to the Wolf River tectonomagmatic event (Medaris et al., 2003).  $^{40}\text{Ar}/^{39}\text{Ar}$  biotite cooling ages from the WRB are only slightly younger than its intrusive age (ranging from 1460 to 1415 Ma) consistent with shallow emplacement (Holm and Lux, 1998; Holm et al., 2007).

The final Proterozoic crust-forming event in the southern Lake Superior region was aborted intracontinental rifting at 1100 Ma that created the Midcontinent Rift System (MRS; Van Schmus and Hinze, 1985; Hinze et al., 1997). MRS magmatism produced a profound magnetic and gravity anomaly that can be traced for 2500 kilometers along an arcuate path across the midcontinent (Fig. 1), with its location in the Lake Superior region influenced by the shape of the Paleoproterozoic (2.3–1.9 Ga) pre-Penokean craton margin (Ola et al., 2016).

### 3. Pre and post-Penokean mafic magmatism

#### 3.1 Pembine ophiolite in northeast Wisconsin

The dismembered Pembine suprasubduction zone ophiolite (Schulz, 1987) is located within the Pembine-Wausau terrane south of the Niagara suture zone in northeastern Wisconsin (locality PO, Fig. 1). As described in LaBerge et al. (2003), the ophiolite is composed of mid-ocean ridge-type basalts and gabbros, primitive island-arc tholeiitic pillow basalt and diabase, boninitic pillowed flows and breccias, and massive to layered peridotite-gabbro bodies locally intruded by sheeted mafic dikes, and ultramafic rocks (pyroxenites and serpentinites). The ophiolite sequence is overlain to the south by low-K calc-alkaline andesite to rhyolite lava flows and volcanoclastic rocks with oceanic-arc compositional characteristics and is intruded by syn-volcanic diorite-quartz diorite-tonalite bodies as well as syn- to post-tectonic diorite-tonalite-granite plutons. One of these, the Twelve Foot Falls quartz diorite, is a large 20 km x 5 km sill-like pluton, which intrudes the upper part of the ophiolite sequence and is in fault contact with calc-alkaline volcanic rocks (Fig. 2; Sims and Schulz, 1993). The quartz diorite is similar in chemical composition to low-K primitive calc-alkaline andesites (Sims et al., 1992).

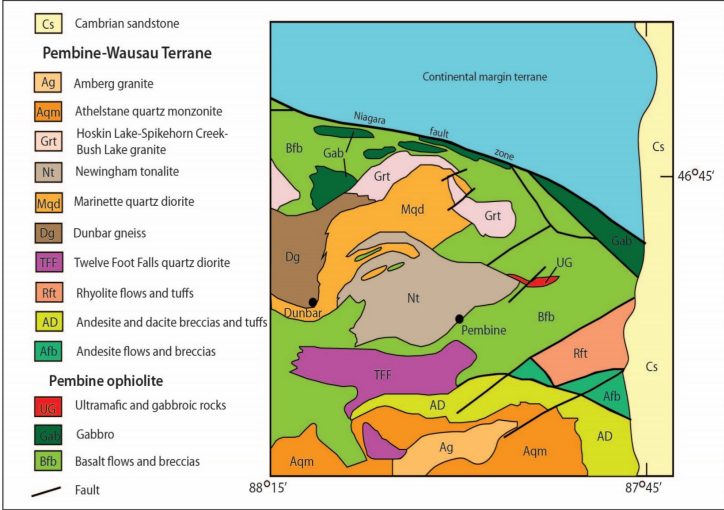


Fig. 2: Simplified geology of the Pembine-Wausau terrane in northeast Wisconsin showing the Pembine ophiolite and Twelve Foot Falls quartz diorite (after Sims and Schulz, 1993).

### 3.2 Mafic dikes of central Wisconsin

Strongly deformed Precambrian rocks exposed along and near the Wisconsin River in central Wisconsin (between Stevens Point and Wisconsin Rapids) occur at the nexus of where the 1475 Ma Wolf River batholith intrudes the Penokean WMT and the Yavapai SLTZ (locality BD, Fig. 1). Precambrian basement in this area consists of Archean tonalitic to dioritic gneiss and migmatite and a variety of Penokean igneous rocks, including tonalite, granodiorite, and granite (Sims et al., 1989; Van Wyck, 1995). Many of the igneous rocks have been re-crystallized, exhibiting a range of planar and linear fabrics. Subvertical east-northeast striking diabase dikes, now recrystallized to amphibolite, intrude the deformed Penokean igneous rocks (Fig. 3; Maass et al., 1980).

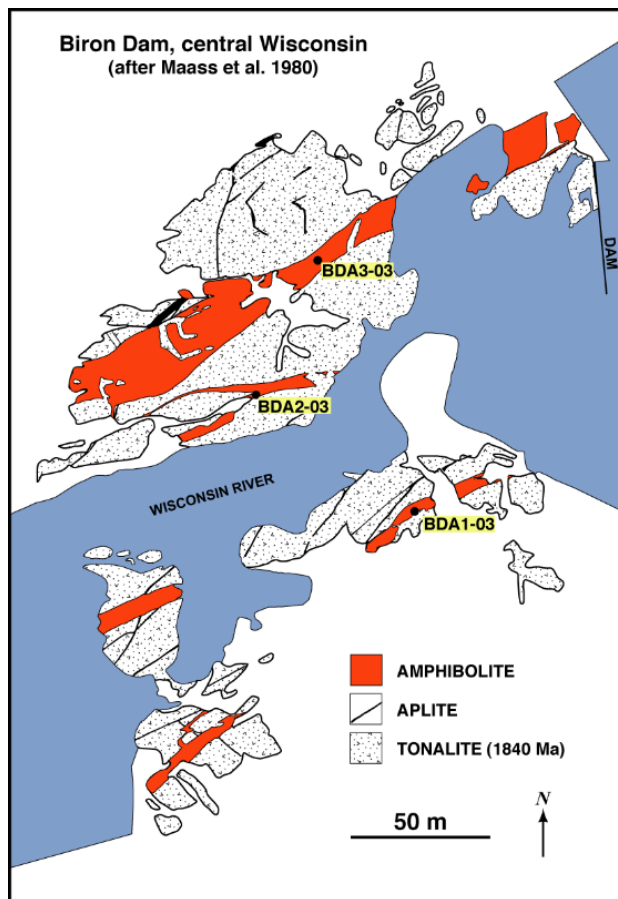


Fig. 3: Geologic map of the Biron dam area, showing the distribution of Penokean tonalite, aplite dikes and metadiabase dikes with sample localities.

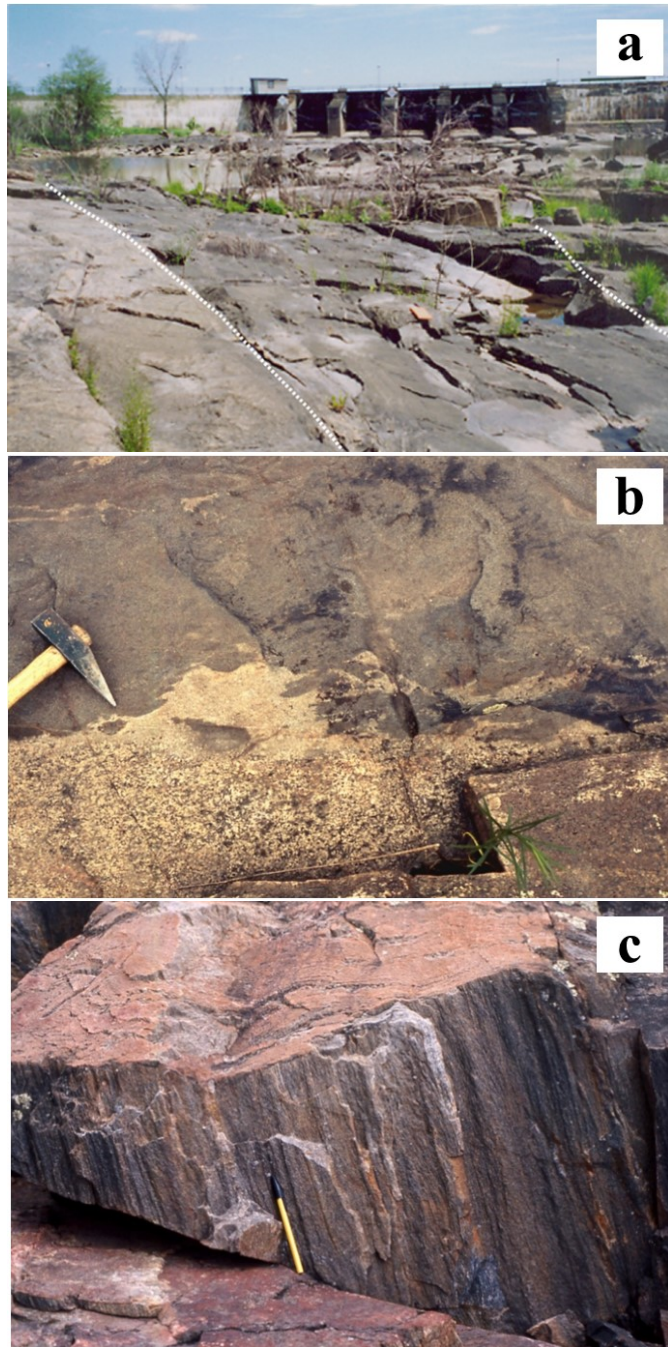


Fig. 4: a) Photo of Biron dam with sharp dike contacts (dotted lines) and tonalite in the foreground. b) Photo of Biron dam dike contact showing partial melting and rheomorphic veining. c) Photo of strongly lineated tonalite at Conants Rapids.

The dike margins have not been severely deformed and maintain sharp cross-cutting contacts with the ca. 1840 Ma Penokean tonalites they intruded (Fig. 4a; Van Wyck, 1995), including local preservation of melting in tonalite at contacts with the metadiabase (Fig. 4b).

The metadiabase dikes are trachybasalt in composition, containing 50.6–51.4 wt% SiO<sub>2</sub> and 5.0–5.3 wt% Na<sub>2</sub>O+K<sub>2</sub>O, and having Mg-numbers (100 x molar MgO/[MgO+FeO]) of 48.6–55.0. Samples collected from three of the dikes are close to silica saturation, with BDA–1 containing 0.46 wt.% normative quartz and BDA–2 and BDA–3 containing 1.15 and 1.20 wt% normative olivine, respectively. In terms of trace elements, the trachybasalt exhibits a pronounced subduction signature that is characterized by negative anomalies for Nb and Ta, Sr, P, Zr and Hf, and Ti, and a strongly positive anomaly for Pb (Fig. 5). With relatively high K<sub>2</sub>O, Th and light REE contents, the trachybasalt most resembles calc-alkaline continental arc basalt (Murphy, 2007).

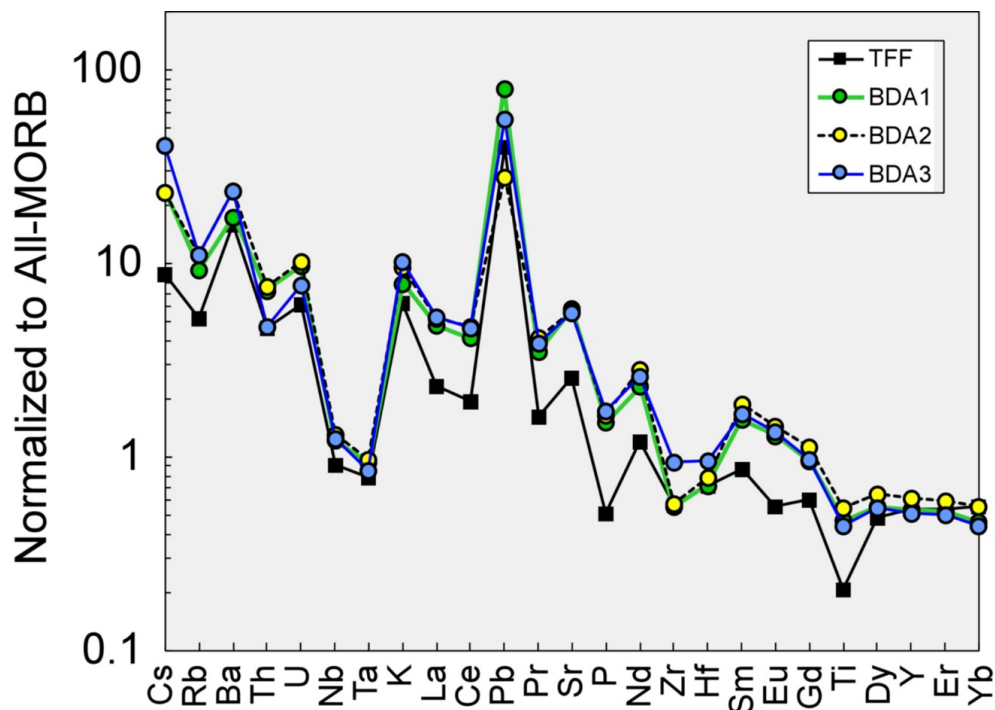


Fig. 5: Extended trace element plot of Twelve Foot Falls quartz diorite and metadiabase dikes at Biron dam, normalized to All-MORB (Gale et al., 2013).

Except for a few unmetamorphosed ca. 1100 Ma MRS diabase dikes, all rock units have been metamorphosed under amphibolite-facies conditions and possess a steeply plunging, penetrative mineral lineation (Fig. 4c). Detailed mapping and structural analysis document three steeply plunging sets of isoclinal to open folds with fold axes that parallel the prominent mineral lineation (Maass et al., 1980). Holm et al. (2007) reported an  $^{40}\text{Ar}/^{39}\text{Ar}$  plateau age of  $1600 \pm 5$  Ma on biotite separated from one of the amphibolite dikes indicating the dikes must be late Paleoproterozoic in age (between 1840 and 1600 Ma).

#### **4. Analytical methods**

##### *4.1 U-Pb geochronology*

Zircon was separated from 2 kg rock samples using standard mineral separation techniques. The handpicked zircon grains were mounted in epoxy and polished and imaged using a scanning electron microscope. All isotopic measurements were made using the CAMECA ims1270 ion microprobe housed within the National Ion Microprobe Facility at the University of California, Los Angeles. The U-Pb measurements were made with a  $\sim 20 \mu\text{m}$   $\text{O}^-$  beam according to the methods of Schmitt et al. (2003) for analyses of polished zircon. Zircon standard AS3 ( $1099 \pm 1$  Ma; Paces and Miller, 1993) was used to determine the relative sensitivities for Pb and U of the unknowns using a calibration technique similar to Compston et al. (1984). U-Pb isotopic ratios and ages were calculated from measured ion intensities, using in-house software written by C.D. Coath (ZIPS v3.4), and are corrected for  $^{204}\text{Pb}$ . Isoplot v3.0 (Ludwig, 2003) was used to plot weighted mean, age probability diagrams and Concordia diagrams. Results are presented in Supplementary Table 1 and Figure 6. Errors on individual spot ages are reported at the  $1\sigma$  level and weighted mean ages are presented at the 95% level of confidence ( $2\sigma$  level) based on the  $^{207}\text{Pb}/^{206}\text{Pb}$  isotopic ratios.

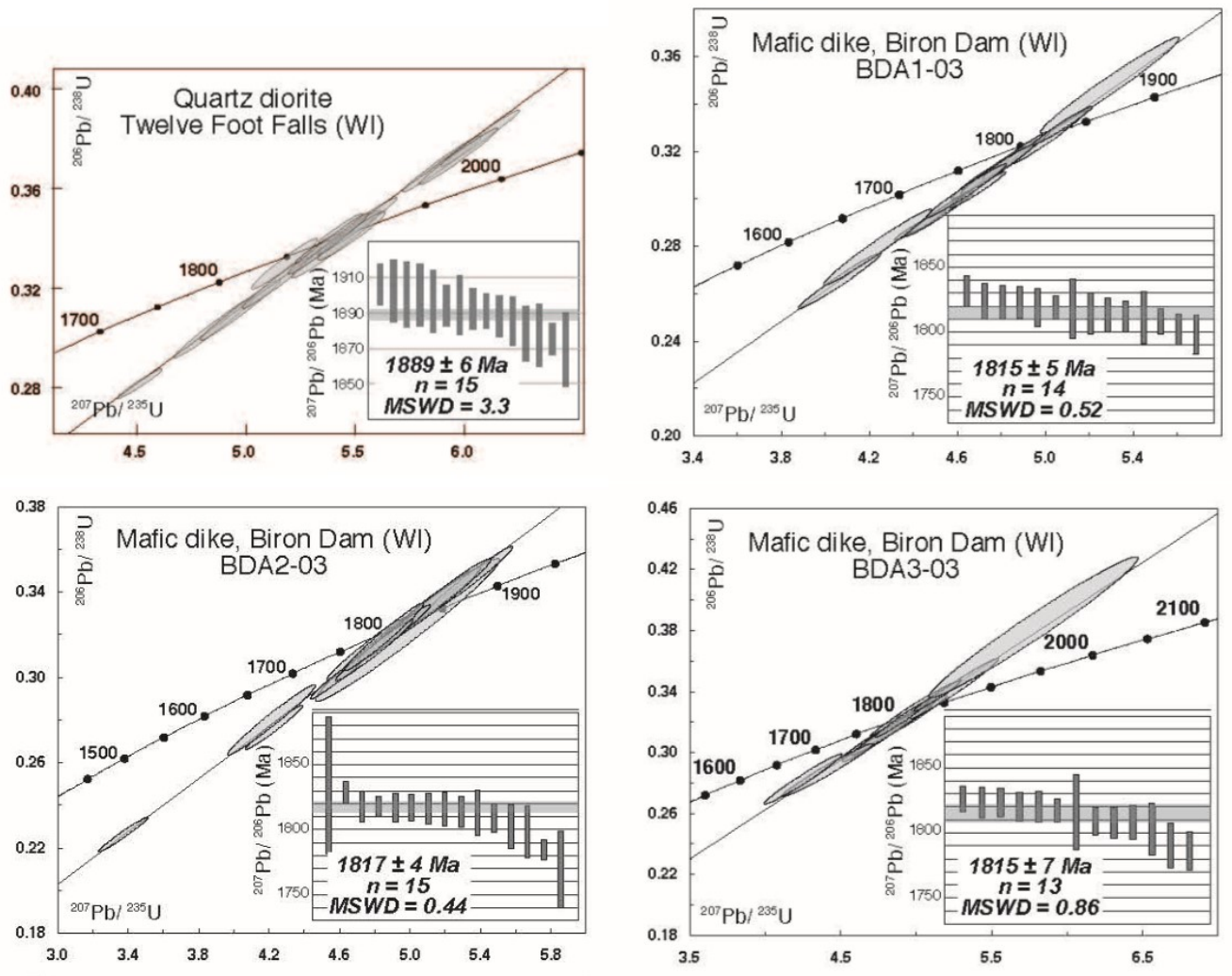


Fig. 6: Zircon U-Pb Concordia plots from Twelve Foot Falls quartz diorite (1889 Ma) and three metadiabase dikes at Biron dam (all 1817 Ma).

#### 4.2 $^{40}\text{Ar}/^{39}\text{Ar}$ thermochronology

$^{40}\text{Ar}/^{39}\text{Ar}$  incremental analyses using a defocused  $\text{CO}_2$  laser beam were performed at the University of Wisconsin Rare Gas Geochronology Laboratory with procedures like those of Smith et al. (2006). Several samples of amphibolite containing medium-grained hornblende, one sample of schist containing muscovite, and two samples of microcline-bearing granite were crushed to 250-500  $\mu\text{m}$ . A few milligrams of hornblende, muscovite, and microcline grains were handpicked and then irradiated in the CLICIT facility (cadmium-shielded) of the Oregon State

University nuclear reactor for 40 h. The conversion efficiency of  $^{39}\text{K}$ - $^{39}\text{Ar}$  was monitored using sanidine from the 28.34 Ma Taylor Creek Rhyolite (Renne et al., 1998). Based on the monitors, the neutron fluence parameter  $J$  is  $0.010402 \pm 0.000052$  ( $2\sigma$ ). Corrections for interfering nuclear reactions are based upon previous measurements on synthetic K-glass and  $\text{CaF}_2$  salts (Supplementary Table 2). A five-grain aliquot of sample was placed in a well on a copper disc and heated 2 min for each gas increment released, with laser output power varying from 1 to 6 W. The released gas was purified for 5 min with two SAES GP-50 getters and admitted into a MAP 215-50 mass spectro-meter for Ar isotope analysis using an electron multiplier. System blanks were measured before and after every three analyses, and data were corrected for blanks and mass-fractionation effects. Final data reduction was via ArArCalc (Koppers, 2002). Results are given in Supplementary Table 2 and Figure 7. The uncertainty in age reflects analytical uncertainties only at the  $2\sigma$  level.

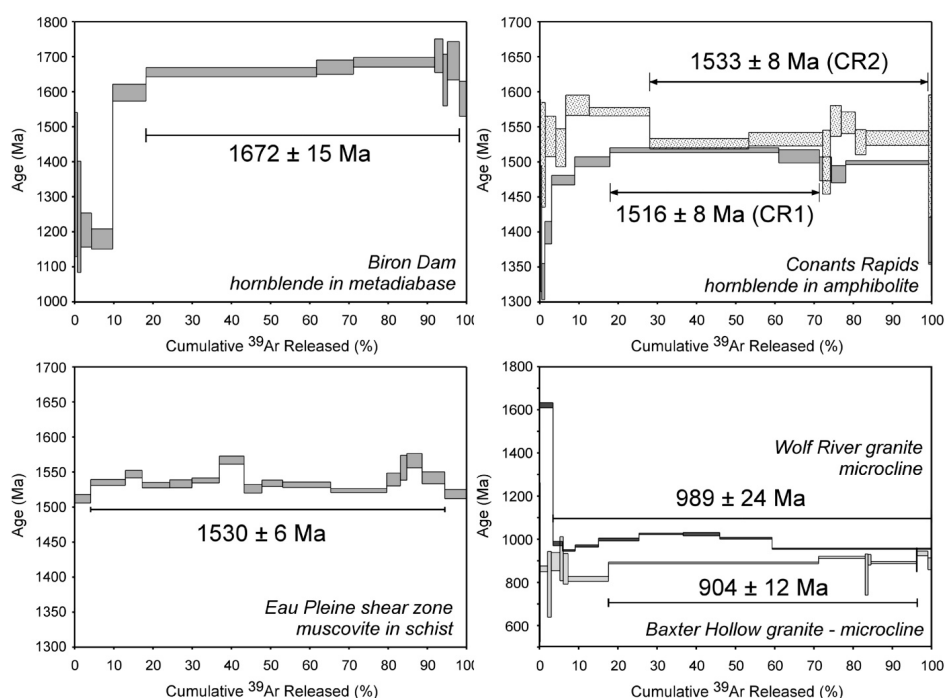


Fig. 7:  $^{40}\text{Ar}/^{39}\text{Ar}$  degassing spectra from central Wisconsin. a) hornblende from metadiabase dike; Biron dam; b) hornblende from amphibolite lenses in Archean gneiss at Conants Rapids <10 km from Wolf River batholith; and c) muscovite from the Eau Pleine shear zone. d) microcline from the 1476 Ma Wolf River granite and 1750 Ma Baxter Hollow granite.

Nominal closure temperatures of 500 °C for hornblende, 350 °C for muscovite, and below 300 °C but above 150 °C for potassium feldspar are used (cf. McDougall and Harrison, 1999).

#### 4.3 $^{40}\text{Ar}/^{39}\text{Ar}$ K-feldspar multi-diffusion domain (MDD) thermochronology

$^{40}\text{Ar}/^{39}\text{Ar}$  analysis of K-feldspar using the MDD method has been utilized in a number of laboratory experiments (Harrison et al., 1991; Lovera et al., 1989, 1993, 1997, 2002) and has recently been successfully applied to link higher and low-temperature thermochronological systems from well-constrained cratonic localities (McDannell et al., 2018).  $^{40}\text{Ar}/^{39}\text{Ar}$  K-feldspar MDD analysis is able to determine continuous temperature-time paths over the range ~150 to ~300 °C.  $^{40}\text{Ar}/^{39}\text{Ar}$  step-heating analyses were performed on potassium feldspar at the Lehigh University noble gas laboratory using the methodology described in McDannell (2017) and McDannell et al. (2018).

Additional samples of granites (described below) were crushed, sieved to 250  $\mu\text{m}$ , and separated using methylene iodide to isolate the feldspar fraction. Approximately 1.0-1.5 mg of feldspar per sample was handpicked and irradiated with K and Ca salts and GA1550 biotite flux monitors at the Oregon State University CLICIT nuclear reactor for 50 h. Samples were outgassed using incremental (isothermal duplicate) step heating by a double-vacuum resistance furnace with a Mo crucible over 54 heating steps from 450-1450 °C, with multiple isothermal steps at 1100 °C to extract as much gas as possible before sample melting. The automated extraction system fitted with SAES GP-50 getters is connected to a Thermo Argus VI multi-collector mass spectrometer operated at 4.5 kV accelerating potential and 200 mA trap current. Under these conditions, the background for  $^{36}\text{Ar}$  is  $1 \times 10^{-14}$  cc STP. Routine Ar analyses are performed in multi-collector mode using Faraday detectors to measure  $^{40}\text{Ar}$ ,  $^{39}\text{Ar}$ ,  $^{38}\text{Ar}$  and  $^{37}\text{Ar}$ ,

and either a fifth Faraday detector or an ion-counting electron multiplier is used to measure  $^{36}\text{Ar}$ . Furnace temperature is monitored by a W-Re thermocouple and a laser extraction line is outfitted with a Merchantek  $\text{CO}_2$  laser operated with a continuous 10.6  $\mu\text{m}$  beam (variable output power up to 35 W) for fusion of Ca and K salts for calculating the mass discrimination factor and mass interferences. The GA-1550 biotite standard ( $98.5 \pm 0.5$  Ma; McDougall and Wellman, 2011) is also outgassed for neutron flux monitoring to determine irradiation constants.

Raw mass spectrometer data are reduced using ArArCalc (Koppers, 2002) and beam values are regressed to the time of gas inlet and corrected for background, line blank, discrimination, decay of  $^{37}\text{Ar}$  and  $^{39}\text{Ar}$ , and Ca and K-derived nucleogenic interferences. All  $^{40}\text{Ar}/^{39}\text{Ar}$  step ages are accompanied by propagation of uncertainties due to line blank, mass discrimination, peak-height regressions, nucleogenic interferences, flux monitor measurements, J-factor interpolation, and decay constants. All raw  $^{40}\text{Ar}/^{39}\text{Ar}$  data discussed below are available from the online repository: <https://preserve.lehigh.edu/etd/2721>.

#### *4.4 Inverse thermal modeling of MDD data*

Data derived from MDD thermochronology (i.e., the sample's specific diffusion kinetics and domain-size distribution) can be used to invert the MDD age spectrum to its thermal history. Inverse thermal history modeling of MDD data was carried out following the methods outlined in McDannell et al. (2018), by first using the *domains* program to invert the laboratory-derived kinetic data and heating schedule for feldspar domain structure. The same approach was taken for each sample when modeling the diffusion domain distribution: (1) use of a slab diffusion geometry; (2) modeling was only performed up to 1050-1100  $^{\circ}\text{C}$ , just before typical K-feldspar melting temperature; (3) the number of diffusion domains were allowed to be between 3 and 10; and (4) The  $E_a$  and  $\log D_0/r^2$  values must all be within the range reported in the large database of

>100 samples by Lovera et al. (1997). After data reduction, samples were only considered for inverse modeling if there was acceptable cross-correlation (Lovera et al., 2002) between the observed age spectrum and the  $\log R/R_0$  spectrum determined from  $^{39}\text{Ar}$  release kinetics: a good correlation ( $>0.9$ ) supports the fundamental requirement that  $^{40}\text{Ar}$  and  $^{39}\text{Ar}$  diffusion are occurring in the same manner. Inversion of the diffusion domain information for thermal history was carried out using the *Arvert* v. 5.11 software (Zeitler, 2004; Harrison et al., 2005) employing random Monte Carlo exploration with the enhanced learning component of the controlled random search (CRS) algorithm (Price, 1977; Willett, 1997). The only imposed *Arvert* model constraints were that maximum heating and cooling rates were required to be  $\leq 2\text{-}3^\circ\text{C}/\text{My}$  and only MDD data were modeled during simulations. The Wolf River batholith sample was also modeled using QTQt v. 5.7 (Gallagher, 2012) utilizing the Bayesian Markov-chain Monte Carlo method for comparison to the CRS results. The QTQt model was a total of 550,000 iterations with the only imposed constraints being maximum allowed rates of  $dT/dt = 2^\circ\text{C}/\text{My}$ , the published biotite  $^{40}\text{Ar}/^{39}\text{Ar}$  data of Holm and Lux (1998) as a high-temperature constraint, and a Cambrian ( $25 \pm 15^\circ\text{C}$  at  $520 \pm 20\text{ Ma}$ ) near-surface constraint, in agreement with the regional preserved stratigraphy.

#### 4.5 Electron microprobe geothermometry

Minerals were analyzed by wavelength-dispersion spectrometry (WDS) with a Cameca SX50 instrument at the University of Wisconsin-Madison. Operating conditions were 15 kV accelerating voltage, 20 nA beam current (Faraday cup) for amphibole and 10 nA for plagioclase, and beam diameter of 1  $\mu\text{m}$  for amphibole and 5  $\mu\text{m}$  for plagioclase. Combinations of natural minerals were used as standards, e.g. amphibole for Si, Al, Fe, Mg, and Ca, rutile for Ti, rhodonite for Mn, jadeite for Na, and microcline for K in unknown amphibole, and natural

oligoclase and andesine for unknown plagioclase. Data reduction was performed by Probe for Windows software, utilizing the  $\phi(\rho z)$  matrix correction of Armstrong (1988). Major element abundances are estimated to be precise within  $\pm 3\%$ , and minor element abundances, within  $\pm 10\%$ , based on replicate analyses. The proportion of ferric iron in amphibole was estimated from charge balance considerations, following the method of Schumacher (1997). Representative amphibole and plagioclase compositions in Biron dam and Conants Rapids metadiabases are given in Table 3.

Table 3. Representative amphibole and plagioclase compositions from 1817 Ma metadiabase dikes

Mineral	Amphibole			Plagioclase			
	Locality	Locality		Locality	Locality		
	<u>Biron Dam</u>	<u>Conants Rapids</u>		<u>Biron Dam</u>	<u>Conants Rapids</u>		
Sample	86GM100	01CR1A	01CR2A	Sample	86GM100	01CR1A	01CR2A
# of analyses	29	25	25	# of analyses	45	45	45
wt. %	wt. %			wt. %			
SiO <sub>2</sub>	42.74	41.68	42.88	SiO <sub>2</sub>	58.10	62.51	62.57
TiO <sub>2</sub>	0.65	0.67	0.58	Al <sub>2</sub> O <sub>3</sub>	26.69	23.27	23.94
Al <sub>2</sub> O <sub>3</sub>	11.40	10.06	9.48	Fe <sub>2</sub> O <sub>3</sub>	0.08	0.09	0.10
FeO <sub>Total</sub>	16.07	20.47	19.13	CaO	8.31	4.65	5.15
MnO	0.29	0.33	0.36	Na <sub>2</sub> O	6.61	8.59	8.21
MgO	10.57	8.38	9.42	K <sub>2</sub> O	0.07	0.20	0.19
CaO	11.67	11.58	11.71	Sum	99.87	99.32	100.15
Na <sub>2</sub> O	1.25	1.25	1.16				
K <sub>2</sub> O	0.62	1.13	1.01	<i>cations per 5 oxygen atoms</i>			
Sum	95.27	95.56	95.73	Si	2.599	2.783	2.763
<i>cations after Schumacher (1997)</i>				Al	1.407	1.221	1.246
<i>T-site</i>				Fe <sup>3+</sup>	0.003	0.003	0.003
Si	6.476	6.473	6.588	Ca	0.398	0.222	0.244
Al IV	1.524	1.527	1.412	Na	0.573	0.742	0.703
Sum	8.0	8.0	8.0	K	0.004	0.011	0.010
<i>C-site</i>				Σ Cations	4.985	4.982	4.969
Al VI	0.513	0.314	0.305	<i>% end members</i>			
Cr	0.000	0.000	0.000	An	40.8	22.8	25.5
Fe <sup>3+</sup>	0.488	0.536	0.507	Ab	58.8	76.0	73.4
Ti	0.075	0.078	0.068	Or	0.4	1.2	1.1
Mg	2.388	1.941	2.157				
Fe <sup>2+</sup>	1.548	2.122	1.951				
Mn	0.038	0.043	0.047				
Sum	5.0	5.0	5.0				
<i>B-site</i>							
Ca	1.895	1.927	1.927				
Na	0.056	0.039	0.039				
Sum	2.0	2.0	2.0				
<i>A-site</i>							
Na	0.253	0.336	0.307				
K	0.119	0.225	0.198				
Sum	0.372	0.561	0.505				
Σ Cations	15.373	15.561	15.506				

## 1 **5. Results**

### 2 *5.1 U-Pb geochronology*

#### 3 *5.1.1 Twelve Foot Falls Quartz Diorite, Pembine, Wisconsin*

4 Previous attempts to date the volcanic components of the Pembine ophiolite were  
5 unsuccessful because of a lack of recoverable zircon, probably caused by the generally low  
6 zirconium content of these primitive arc rocks. However, we were able to separate magmatic  
7 zircons from the Twelve Foot Falls quartz diorite, a gray, generally medium- to coarse-grained  
8 quartz diorite containing crystals of subhedral sodic andesine, subhedral hornblende, and  
9 anhedral bluish quartz (Sims et al., 1992).

10 Zircon grains are colorless and mostly doubly terminated euhedral grains. A total of 15  
11 spots on nine zircon grains were analyzed. The Th/U values are generally <0.5. The ages range  
12 from 1875 to 1905 Ma that define a discord with a weighted mean  $^{207}\text{Pb}/^{206}\text{Pb}$  age of  $1889 \pm 6$   
13 Ma (MSWD: =3.3; Fig. 6a and Supplementary Table 1).

14

#### 15 *5.1.1 Metadiabase dikes, central Wisconsin*

16 Three amphibolitized mafic dikes were sampled along the Wisconsin River below Biron  
17 dam, ~ 6 kilometers north of Wisconsin Rapids (Fig. 3). The dikes are black and fine- to  
18 medium-grained and interpreted to be metamorphosed diabase intrusions (Maass et al.,  
19 1980). The mineralogy of the dikes consists of plagioclase ( $\text{An}_{41}$ ) + amphibole  
20 (magnesiohornblende) + titanite + apatite ± biotite ± epidote ± quartz. Steeply aligned amphibole  
21 grains define a strong nematoblastic fabric.

22 Separated zircon grains are pink and mostly subhedral with slight overgrowths. The  
23 results for the three samples are plotted on Concordia diagrams (Fig. 6 b, c, d) and the isotopic

24 analyses are given in Supplementary Table 1. Age data are reported as  $^{207}\text{Pb}/^{206}\text{Pb}$  ages and were  
25 used to calculate weighted averages. Like the quartz diorite that was dated, the Th/U values are  
26 quite low.

27 A total of 14 spots on twelve zircon grains from sample BDA1-03 were analyzed. The ages  
28 range from ca. 1830 to 1800 Ma with a weighted mean  $^{207}\text{Pb}/^{206}\text{Pb}$  age of  $1815 \pm 5$  Ma (MSWD:  
29 0.52) for all spots. A total of 15 spots on 14 zircon grains from BDA2-03 were analyzed, with  
30 ages ranging from about 1830 to 1770 Ma with a weighted mean  $^{207}\text{Pb}/^{206}\text{Pb}$  age of  $1817 \pm 4$  Ma  
31 (MSWD: 0.44) for all 15 spots.

32 A total of 13 spots on ten zircon grains from BDA3-03 were analyzed yielding ages from  
33 ca. 1830 to 1790 Ma and resulting in a weighted mean  $^{207}\text{Pb}/^{206}\text{Pb}$  age of  $1815 \pm 7$  Ma (MSWD:  
34 0.86) for all 13 spots. The weighted mean ages for the three samples all fall within error of each  
35 other and when combined result in weighted mean  $^{207}\text{Pb}/^{206}\text{Pb}$  age of  $1817 \pm 2$  Ma with an  
36 MSWD of 0.70.

37

### 38 5.2 $^{40}\text{Ar}/^{39}\text{Ar}$ thermochronology

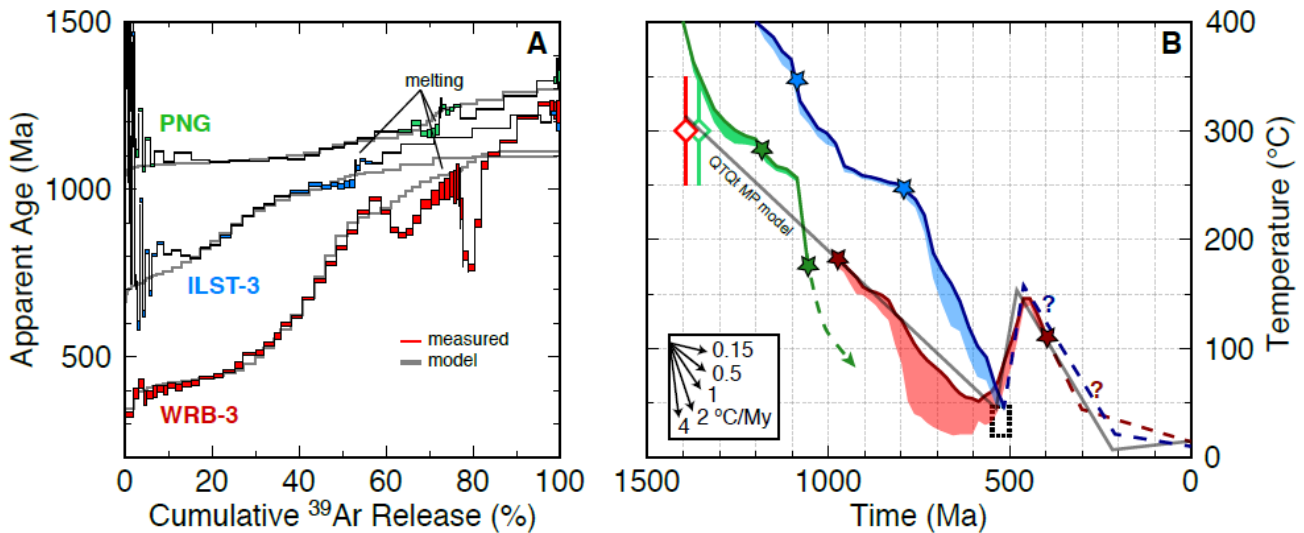
39  $^{40}\text{Ar}/^{39}\text{Ar}$  laser step-heating of hornblende from a metadiabase dike at Biron dam (the same  
40 locality from which we obtained U-Pb zircon ages) yields a plateau age of  $1672 \pm 15$  Ma for over  
41 80% of the gas released (Fig. 7a). Biotite from metadiabase at Biron dam previously yielded a  
42 plateau age of  $1600 \pm 5$  Ma (Holm et al., 2007). At Conants Rapids, ~17 km northeast of Biron  
43 dam, amphibolite occurs as slightly folded metadiabase dikes cross-cutting Archean gneiss and  
44 1842 Ma foliated and lineated tonalites (Maass et al., 1980; Sims et al., 1989). Laser step-heating  
45 of hornblende from two of these mafic dikes yields plateau ages of  $1516 \pm 8$  Ma and  $1533 \pm 8$   
46 Ma (Fig. 7b). Muscovite in low-grade schist, which was collected from the Eau Pleine shear zone

47 35 km north of Biron dam, yields an  $^{40}\text{Ar}/^{39}\text{Ar}$  plateau age of  $1530 \pm 6$  Ma for >90% of the gas  
48 released (Fig. 7c). Lastly, microcline separates from the Wolf River granite (location WRB, Fig.  
49 1) and from the Baxter Hollow granite (sample BHG located in the Baraboo Range, Fig. 1)  
50 yielded Ar/Ar plateau ages of  $989 \pm 25$  Ma and  $904 \pm 12$  Ma respectively (Fig. 7d).

51

### 52 5.3 $^{40}\text{Ar}/^{39}\text{Ar}$ MDD thermochronology

53 Potassium feldspar separates were obtained from three Proterozoic granites for  $^{40}\text{Ar}/^{39}\text{Ar}$   
54 MDD analysis: the Penokean Neillsville granite (location PNG; Sims 1993), the geon 14 Wolf  
55 River granite (location WRB-3), and a geon 14 granite core sample from deep borehole UPH-3  
56 (Hoppe et al., 1983) from the Illinois basement just south of Wisconsin (location ILST-3).  
57 Samples PNG and ILST-3 show evidence of excess Ar during early  $^{39}\text{Ar}$  release. Furnace heating  
58 of K-feldspar from Wolf River granite sample WRB-3 (biotite  $^{40}\text{Ar}/^{39}\text{Ar}$  age of ca. 1392 Ma;  
59 Holm and Lux, 1998) yields step ages ranging from ca. 970-380 Ma and an age spectrum  
60 indicative of slow cooling. The age spectrum shows plausible evidence of large diffusion domain  
61 breakage from crushing or minor recrystallization but yields an excellent  $\log R/R_0$  cross-  
62 correlation of 0.99 (Fig. 8a). However, this sample is characterized by a low activation energy of  
63  $\sim 159$  kJ/mol, which is within the range of  $E_a$  reported in Lovera et al. (1997) but is below the  
64 'typical' K-feldspar  $E_a$  of  $\sim 170$ -210 kJ/mol (Reiners et al., 2005).



65 Fig. 8:  $^{40}\text{Ar}/^{39}\text{Ar}$  age spectra and thermal history simulations for feldspar samples PNG,  
 66 ILST-3, and WRB-3. (A) Age spectra showing apparent age vs. cumulative  $^{39}\text{Ar}$  release.  
 67 Measured age spectra (red) and Arvert model spectra (cyan). (B) Time-temperature plots  
 68 showing Arvert model thermal history envelopes. Envelopes are T-t path bundle  
 69 encompassing 150 T-t paths with the best-fitting path shown by heavy colored line. Gray  
 70 line is the QTQt maximum posterior T-t history (Bayesian preferred model) for WRB-3  
 71 that is similar to the Arvert solution set. Dotted box is the Cambrian constraint used in  
 72 the QTQt model. Modeled histories in panel B produce the model spectra in panel A. The  
 73 stars denote the portion of the T-t path constrained by the Ar MDD data. Dashed lines  
 74 are inferred T-t paths. Diamonds are published biotite  $^{40}\text{Ar}/^{39}\text{Ar}$  data for PNG and WRB-  
 75 3 with respective closure temperature range for the system.

76  
 77  
 78 Feldspar sample PNG (biotite  $^{40}\text{Ar}/^{39}\text{Ar}$  plateau age of ca. 1357 Ma; Romano et al., 2000)  
 79 exhibits apparent step ages ranging from ca. 1170 Ma to 1080 Ma and an age spectrum indicative  
 80 of rapid cooling (Fig. 8a). The age spectrum for sample ILST-3 is characterized by step ages  
 81 from ca. 1015-795 Ma. The late  $^{39}\text{Ar}$  release (~45-52%) indicates relatively rapid cooling due to  
 82 a plateau-like portion of the age spectrum that yields a weighted mean age of  $1012.41 \pm 1.46$  Ma  
 83 ( $2\sigma$ ; MSWD: 1.46, n: 6), followed by staircase-pattern step ages indicative of slow cooling (17-  
 84 42% release) from 975 to 800 Ma.

85 Low temperature thermal history simulations of the MDD feldspar spectra suggest  
 86 regionally variable lower temperature resetting and/or cooling of the Penokean and Yavapai

87 provinces in the Neoproterozoic. Time-temperature plots showing *Arvert* model thermal history  
88 envelopes for feldspar samples PNG, ILST-3, and WRB-3 are shown in Fig. 8b. The stars denote  
89 the portion of the T-t path constrained by the Ar MDD data. Inferred T-t paths depicted by  
90 dashed lines are discussed below.

91

#### 92 *5.4 Amphibole-Plagioclase geothermometry*

93 Holland and Blundy (1994) have formulated geothermometers for two amphibole-  
94 plagioclase equilibria:

95 1) edenite + 4quartz = tremolite + albite, and

96 2) edenite + albite = richterite + anorthite.

97 Following these formulations, coexisting magnesiohornblende and andesine in metadiabase at  
98 Biron dam yield 725 °C and 658 °C for equilibria 1 and 2, respectively, at an assumed pressure of  
99 6 kb (Table 4; the pressure dependence for equilibrium 1 is -1 °C/kb and for equilibrium 2 is +7  
100 °C/kb). Of these two equilibria, the first is more appropriate, because metadiabase is close to  
101 being silica saturated, as previously described.

102 Two samples of amphibolite at Conants Rapids yield similar results for the same two  
103 equilibria, these being 713-725 °C and 628-632 °C, in this case for coexisting pargasite and  
104 oligoclase, again calculated for an assumed pressure of 6 kb. The pressure dependence in this  
105 case is -7 °C/kb for equation 1 and +4 °C/kb for equation 2.

Table 4. Temperature estimates for coexisting amphibole and plagioclase in Biron dam metadiabase and Conants Rapids amphibolite

Locality	Biron Dam	Conants Rapids	
Sample	86GM100	01CR1A	01CR2A
Equation A: edenite-tremolite			
P (kb) 2	729	751	739
6	725	725	713
10	722	698	686
Equation B: edenite-richterite			
P (kb) 2	630	617	612
6	658	632	628
10	686	648	643

## 106 6. Discussion

### 107 6.1 Minimum age of the Pembine ophiolite

108 The  $1889 \pm 6$  Ma date for the Twelve Foot Falls quartz diorite sill provides a minimum age  
109 for the Pembine ophiolite and confirms that the ophiolitic sequence is older than most Paleo-  
110 proterozoic rocks in the Pembine-Wausau magmatic terrane (mostly 1875-1835 Ma) and formed  
111 at least 30 m.y. before accretion of the Pembine-Wausau magmatic terrane to the southern  
112 margin of the Superior craton along the Niagara suture zone at ca. 1860 Ma. Several  
113 Paleoproterozoic mafic dike swarms, including the Marathon, Kapuskasing, Fort Frances, and  
114 recently identified dikes in northern Michigan (Schulz et al., 2018), are all ca. 2100 Ma and  
115 appear to mark the time of final rifting along the southern margin of the Superior craton (Halls et  
116 al., 2008; although Pietrzak-Renaud and Davis [2014] suggest at least local extension was  
117 occurring north of the Niagara Fault zone ca. 1890 Ma). Thus, there is approximately a 200 m.y.  
118 hiatus between rifting of the late Archean supercontinent Kenorland (Williams et al., 1991) and  
119 formation of the Pembine ophiolite before 1890 Ma and its obduction during Penokean island arc  
120 accretion along the Niagara fault zone. The new minimum age for the Pembine ophiolite  
121 suggests that a Paleoproterozoic ocean basin evolved following rifting of Kenorland at about

122 2200-2100 Ma, and that subduction systems in this ocean led to the generation of new arc crust  
123 and repeated accretion events along a Pacific-type southern margin of the Superior craton  
124 (Schulz and Cannon, 2007).

125

## 126 *6.2 Origin of metadiabase dikes in the Penokean Province*

127 The morphology of the zircon grains from the Biron dam metadiabase dikes and their low  
128 Th/U ratios suggest the zircons are magmatic in origin (Parrish, 1990). In addition, the 650-700  
129 °C peak metamorphic conditions reached by these mafic rocks are below those required to  
130 produce new growth of zircon, and the basement arc rocks into which they intrude are 1840 Ma  
131 or older (Maass et al., 1980). Thus, we interpret the new ca. 1817 Ma U-Pb dates of these dikes  
132 to document an episode of mafic magmatism shortly after the end of Penokean orogenic  
133 magmatism (1835 Ma) and prior to the onset of Yavapai subduction-related magmatism  
134 beginning around 1800 Ma. The pronounced subduction signature exhibited by trace elements in  
135 the dikes reflects derivation from mantle that was previously involved in Penokean subduction  
136 and arc accretion. The ca. 1813 Ma Hines quartz diorite that intrudes the Mountain shear zone in  
137 northeast Wisconsin (U-Pb zircon; Sims et al., 1990) and the 1813 ± 5 Ma Wissota dam tonalite  
138 (locality WD, Fig. 1, U-Pb zircon; Craddock et al., 2018) are the only other igneous ages  
139 reported in the 1835-1805 Ma interval (Sims et al., 1990).

140 The Biron dam mafic dikes strike east-northeast, normal to the overall Penokean  
141 convergence direction. Assuming they have not been significantly rotated since they were  
142 emplaced, their current orientation may suggest that these dikes represent a relaxation of  
143 Penokean northwest directed compression and a change to short-lived extensional tectonics,  
144 perhaps in the backarc region of a northwest-directed subducting slab. A similar interpretation of

145 back-arc extension preceding accretion has been proposed for the Penokean orogeny (Schneider  
146 et al. 2002; Schulz and Cannon, 2007). If so, this change to short-lived NW-SE extension may be  
147 the result of initiation of northwest subduction of Yavapai oceanic lithosphere beneath the  
148 accreted Marshfield terrane after Penokean orogenesis. Continued northwest-directed Yavapai  
149 subduction resulted in geon 17 magmatic activity into the Penokean province between 1805 and  
150 1750 Ma prior to accretion of the Yavapai arc terrane during southward growth of the southern  
151 Laurentian margin (Holm et al., 2005; Van Schmus et al., 2007).

152

### 153 *6.3 Age and extent of Proterozoic metamorphism and deformation in central Wisconsin*

154 Our ca. 1817 Ma U-Pb zircon ages from the mafic dikes indicate that the amphibolite  
155 facies metamorphism and fabrics preserved at this locality in central Wisconsin must post-date  
156 Penokean orogenesis (Maass et al., 1980). Given the strong ductile deformation overprint  
157 exhibited in these rocks, it is critical to ascertain whether such overprinting was due to Yavapai,  
158 Mazatzal, or possibly even Wolf River associated tectonism (Schwartz et al., 2018). Published  
159 and new thermochronologic data presented here can help to correctly assign the age of tectono-  
160 metamorphic overprinting.

161 Our younger  $^{40}\text{Ar}/^{39}\text{Ar}$  hornblende ages of ca. 1520-1530 Ma were obtained from  
162 samples collected at Conants Rapids, just 6-7 km from the western exposed edge of the 1470-  
163 1476 Ma Wolf River batholith, and our 1530 Ma  $^{40}\text{Ar}/^{39}\text{Ar}$  muscovite age was obtained from a  
164 quarry within the EPSZ located 10-11 km from the Wolf River batholith. Holm et al. (2007)  
165 obtained three similarly young plateau or near-plateau  $^{40}\text{Ar}/^{39}\text{Ar}$  hornblende ages (1514, 1438,  
166 and 1439 Ma) from country rock also collected near (<10-15 km) the Wolf River batholith.  
167 Together, these are the youngest hornblende cooling ages reported across the entire southern

168 Lake Superior region, and likely reflect the thermal effects of Wolf River magmatism upon the  
169 adjacent country rock, which has witnessed partial resetting of Ar systematics.

170 The 1672 Ma hornblende plateau age from metadiabase at Biron dam, located ~20 km from  
171 the Wolf River batholith, was likely not affected by Wolf River plutonism. Two independent  
172 lines of evidence support this interpretation. First, both theoretical time-governing equations on  
173 the thermal imprint of shallow level plutons (Carslaw and Jaeger, 1959) and direct field tests on  
174 large *shallow* intrusive bodies (i.e., the classic study by Hanson et al., 1975, on the extent of  
175 thermal effects of the Duluth gabbro on Archean country rock in northeastern Minnesota)  
176 indicate a spatially limited thermal aureole of ~10-12 km. Second, the 1600 Ma  $^{40}\text{Ar}/^{39}\text{Ar}$  biotite  
177 plateau age (Holm et al., 2007) from the Biron dam locality falls within a tight cluster of <1620  
178 Ma (1614-1576 Ma) mica  $^{40}\text{Ar}/^{39}\text{Ar}$  plateau ages obtained over a large area of western Wisconsin  
179 – and up to distances of 170 km from the western edge of the exposed batholith. This uniformity  
180 of mica ages represents dominantly low-temperature (350-450 °C) Mazatzal-related resetting  
181 (Holm et al., 1998b; Romano et al., 2000), associated with widespread greenschist-facies  
182 metamorphism of most of the Wisconsin Magmatic terranes. Such low-grade geon 16  
183 metamorphism is also pervasive in the 1750 Ma Montello batholith within the Yavapai terrane  
184 south of the WMT. Although granites and rhyolites in the Montello batholith preserve igneous  
185 structures on macro– and mesoscopic scales, they have been thoroughly recrystallized on the  
186 microscopic scale to albite-bearing greenschist facies mineral assemblages, and the Montello  
187 granite yields a whole-rock Rb–Sr isochron age of 1653 Ma (Van Schmus et al., 1975). The  
188 preservation of a 1600 Ma biotite  $^{40}\text{Ar}/^{39}\text{Ar}$  plateau age at Biron dam is consistent with our  
189 interpretation that the Wolf River batholith did not thermally affect these rocks. Only bedrock  
190 mica  $^{40}\text{Ar}/^{39}\text{Ar}$  ages that are younger than ca. 1600 Ma, such as geon 14–15 ages near the Wolf

191 River batholith and a few geon 11–12 ages north and west of the Wolf River batholith likely  
192 represent thermal resetting of previously Mazatzal reset micas. The 1672 Ma  $^{40}\text{Ar}/^{39}\text{Ar}$  plateau  
193 age obtained here for Biron Dam hornblende, thus likely represents partial isotopic resetting of  
194 hornblende during Mazatzal greenschist-facies metamorphism.

195 We suggest that the 1817 Ma metadiabase dikes were initially deformed and  
196 metamorphosed under amphibolite facies conditions during the Yavapai orogeny, given that they  
197 intruded after Penokean orogenesis and experienced isotopic resetting during Mazatzal  
198 orogenesis. Holm et al. (2007) obtained a metamorphic monazite Pb–Pb age of  $1744 \pm 3$  Ma  
199 from a coarse-grained garnet-staurolite schist in central Wisconsin (Hamburg Schist, locality HS,  
200 Fig. 1) and Van Wyck (1995) reported a preliminary 1722 Ma U–Pb titanite age on a  
201 metadiabase dike cutting a 1851 Ma granodiorite five km west of Biron dam. Additionally,  
202 Romano et al. (2000) obtained a  $1733 \pm 6$  Ma hornblende  $^{40}\text{Ar}/^{39}\text{Ar}$  plateau age in western  
203 Wisconsin. These data provide direct evidence for the existence of a late geon 17 middle  
204 amphibolite facies metamorphic episode in central Wisconsin. Our dike hornblende-plagioclase  
205 geothermometry data suggests Yavapai metamorphic temperatures reached as high as  $\sim 700$  °C in  
206 this part of central Wisconsin. Strong folding with steeply plunging axes and a pervasive steep  
207 mineral lineation (Fig. 4c) can be attributed to the proximity of these rocks to the Spirit Lake  
208 tectonic zone, a Yavapai paleosuture (Fig. 1). A similar structural style of deformation marked  
209 by tight folds with steeply plunging axes in strata just north of the Niagara fault zone in northeast  
210 Wisconsin formed during earlier Penokean arc accretion (Larue, 1983).

211 *6.4 Reheating and Stabilization of Proterozoic lithosphere*

212 Conventional  $^{40}\text{Ar}/^{39}\text{Ar}$  microcline plateau ages of ca. 1000 and 900 Ma (Fig. 7d) suggest  
213 the 1900-1700 Ma accreted Paleoproterozoic terranes finally cooled below 250 °C after 1100 Ma  
214 following extensive plume heating, volcanism, and associated widespread magmatic  
215 underplating during the MCR event.  $^{40}\text{Ar}/^{39}\text{Ar}$  MDD feldspar thermochronology results yield  
216 more complex spectra signifying either slow cooling or resetting of MDD systematics during the  
217 MRS event. For instance, MDD results indicate the post-emplacement thermal history for the  
218 Wolf River batholith consisted of monotonic slow cooling of  $\sim 0.5^\circ\text{C}/\text{Ma}$  throughout the late  
219 Proterozoic (Fig. 8b). Time-temperature histories suggest slow cooling continued to near-surface  
220 conditions of  $\sim 45^\circ\text{C}$  by the early Cambrian, followed by Sauk transgression and Cambro-  
221 Ordovician heating of up to  $\sim 150^\circ\text{C}$  or  $\sim 3.17\text{-}4.75$  km of Paleozoic burial (assuming 20-30  
222  $^\circ\text{C}/\text{km}$  geothermal gradients and  $10^\circ\text{C}$  surface temperature; Fig. 8b). In contrast, feldspar sample  
223 PNG to the west of the Wolf River batholith (Fig. 1) likely experienced post-intrusion slow  
224 cooling through  $\sim 300^\circ\text{C}$ , followed by rapid cooling of  $>4^\circ\text{C}/\text{Ma}$  at ca. 1100 Ma (Fig. 8b). Our  
225 southernmost sample (ILST-3) also shows rapid cooling ca. 1100 Ma, then slow cooling likely  
226 related to prolonged upper-crustal residence (1000-800 Ma) followed by more rapid cooling  
227 during the late Neoproterozoic.

228 Recent reconstructions of intermediate-temperature thermal histories of portions of the  
229 southern Canadian Shield suggest some amount of prolonged mid-crustal residence followed by  
230 significant ( $>5$  km) exhumation at or after ca. 1.0 Ga caused by crustal thickening and isostatic  
231 uplift due to magmatic underplating (McDannell et al., 2018). Our inverse MDD modeling  
232 results provide additional thermal history information from Proterozoic provinces south of the  
233 Archean Superior Province, allowing for comparison of the effects of widespread MRS

234 magmatic underplating on Archean versus Proterozoic continental lithosphere. Although the  
235 currently exposed levels of both Archean and Proterozoic crust of the southern Canadian Shield  
236 display cooling at ca. 1.0 Ga, we interpret cooling of the Proterozoic province rocks to be related  
237 primarily to reheating of already shallow upper-crustal levels, not to exhumation of mid-crustal  
238 levels. The Baldwin conglomerate, which is intruded by the WRB, contains geon 14 detrital  
239 zircon grains indicating shallow conditions of batholith emplacement and limited exhumation of  
240 the region since geon 14 (Medaris et al., 2019). Shallow intrusion is consistent with rapid cooling  
241 of the batholith through  $\sim 300$  °C, with limited metamorphic overprinting of the surrounding  
242 country rock (as described above for the Biron dam locality), and with the presence of miarolitic  
243 cavities in evolved plutons in the batholith (Anderson, 1980). Additionally, the presence of MRS  
244 dike swarms and evidence for localized resetting of  $^{40}\text{Ar}/^{39}\text{Ar}$  isotopic systems further supports  
245 limited post-geon 14 exhumation of this region (Holm et al., 2007). The geologic evidence and  
246 country rock proximity to MRS rifting strongly favors early Neoproterozoic reheating of the  
247 shallow crust, rather than cooling via widespread exhumation as proposed for much of the  
248 Superior Province to the north (McDannell et al., 2018).

249

## 250 **7. Conclusions**

251 Our 1890 Ma zircon age for the Twelve Foot Falls quartz diorite sill near the Niagara  
252 suture zone demonstrates that the Pembine ophiolite formed at least 30 m.y. before its obduction  
253 during accretion of the Pembine-Wausau magmatic terrane. This minimum age is over 200 m.y.  
254 younger than rifting of Kenorland along the southern continental margin, indicating the  
255 likelihood of formation and closure of a major Paleoproterozoic ocean basin.

256 We identify a 30 m.y. gap in orogenic felsic magmatism following the Penokean orogeny  
257 during which only more mafic magmatism is documented (quartz diorite and diabase). We  
258 suggest that the 1835-1805 Ma interval in the southern Lake Superior region represents a  
259 fundamental period of tectonic switching (Collins, 2002) after the Penokean orogeny, when  
260 mafic magmatism was generated in an extensional back-arc setting during the initiation of north-  
261 directed Yavapai subduction. Subsequent 1805-1750 Ma metaluminous to peraluminous granitic  
262 magmatism could be related to a slab window or slab breakoff event during Yavapai subduction.

263 Until recently, metamorphic and deformational fabrics preserved in central Wisconsin  
264 have been attributed solely to Penokean orogenesis. However, our results indicate that the mafic  
265 dikes at Biron dam and Conants Rapids and their Penokean and Archean host rocks were  
266 strongly ductilely deformed at temperatures of  $\sim 700$  °C during 1750-1720 Ma accretion of the  
267 Yavapai arc onto Penokean/Archean rocks along the Spirit Lake tectonic suture. Younger  
268 widespread medium temperature (300-400 °C) isotopic resetting occurred during Mazatzal  
269 regional metamorphic overprinting at 1650-1600 Ma. Geon 14 thermal overprinting was  
270 primarily restricted to a relatively narrow (10-15 km) contact zone surrounding the Wolf River  
271 batholith, consistent with its shallow depth of intrusion. Our results document that portions of the  
272 southern Penokean orogen preserve pervasive Yavapai structures, textures, and mineralogical  
273 compositions. Detailed, comprehensive investigations are needed to properly attribute variations  
274 in strain, structural style, and metamorphic overprinting to specific Proterozoic tectonomagmatic  
275 events in the northern US midcontinent region (Holm et al., 2007; Craddock et al., 2018).

276 At ca. 1.0 Ga, relatively young Proterozoic continental lithosphere of southern Laurentia  
277 was extensively underplated by mafic magmatism, which may have ultimately contributed to its

278 stabilization. In contrast, magmatic underplating of already stabilized Archean Superior Province  
279 lithosphere to the north caused it to be ‘destabilized’ and to undergo widespread exhumation.

280

## 281 **Acknowledgments**

282 This research was funded in part by National Science Foundation grant EAR-027432. We thank  
283 Bill Cannon and John Craddock for reviewing this manuscript.

284

## 285 **Appendix A. Supplementary data**

286 Supplementary Tables 1 and 2 associated with this article can be found online at  
287 <https://doi.org/10.1016/j.jprecamres.2019.105587>.

288

## 289 **References**

290 Anderson, R., 1983. Proterozoic anorogenic granite plutonism of North America. *Geol. Soc. Am.*  
291 *Memoir* 161, 133-152.

292 Armstrong, J.T., 1988. Quantitative analysis of silicates and oxide minerals: comparison of  
293 Monte-Carlo, ZAF and Phi-Rho-Z procedures: p. 239, in: *Proc. Microbeam Analysis*  
294 *Society*, ed. By D.E. Newbury, San Francisco Press, San Francisco.

295 Carslaw, H.S., J.C. Jaeger, 1959. *Conduction of heat in solids*. 2nd ed. Oxford University Press,  
296 New York.

297 Chichester, B., Rychert, C., Harmon, N., van der Lee, S., Frederiksen, A., Zhang, H., 2018.  
298 Seismic Imaging of the North American Midcontinent Rift Using S-to-P Receiver  
299 Functions: Journal of Geophysical Res: Solid Earth, 123. Doi.org/10.1029/2018JB015771.

300 Collins, W.J., 2002. Hot orogens, tectonic switching, and creation of continental crust. *Geology*  
301 30, 535-538.

302 Compston, W., Williams, I.S., Meyer, C., 1984. U–Pb geochronology of zircons from lunar  
303 breccia 73217 using a sensitive high mass-resolution ion microprobe. *J. Geophysical Res.*  
304 (Suppl. 89), B525–B534.

305 Craddock, J.P., Malone, D.H., Schmitz, M.D., Gifford, J., 2018. Strain Variations across the  
306 Proterozoic Penokean Orogen, USA and Canada: *Precambrian Res.* 318, 25-69.

307 Dewane, T.J., Van Schmus, W.R., 2007. U-Pb geochronology of the Wolf River batholith, north-  
308 central Wisconsin: Evidence for successive magmatism between 1484 Ma and 1470 Ma.  
309 *Precambrian Res.* 157, 215-234.

310 Dott, R.H., Jr., 1983. The Proterozoic red quartzite enigma in the north central United States:  
311 resolved by plate collision? *Geol. Soc. Am. Memoir* 160, 129-141.

312 Gale, A., Dalton, C.A., Langmuir, C. II, Su, Y., Schilling, J.–G., 2013. The mean composition of  
313 ocean ridge basalts: *Geochemistry Geophysics Geosystems* 14, 489–518.

314 Gallagher, K., 2012. Transdimensional inverse thermal history modeling for quantitative  
315 thermochronology. *J. Geophysical Res.: Solid Earth* 117(B2).

316 Geiger, C., Guidotti, C., 1989. Precambrian metamorphism in the southern Lake Superior region  
317 and its bearing on crustal evolution. *Geosci. Wisc.* 13, 1-13.

318 Halls, H.C., Davis, D.W., Stott, G.M., Ernst, R.E., Hamilton, M.A., 2008, The Paleoproterozoic  
319 Marathon large igneous province: New evidence for a 2.1 Ga long-lived mantle plume event  
320 along the southern margin of the North American Superior Province: *Precambrian Res.* 162,  
321 327-353.

322 Hanson, G.N., K.R. Simmons, A.E. Bence, 1975, Ar/Ar spectrum ages for biotite, hornblende  
323 and muscovite in a contact metamorphic zone: *Geochim. Cosmochim. Acta* 39, 1269-1277.

324 Harrison, T.M., Lovera, O.M., Heizler, M.T., 1991.  $^{40}\text{Ar}/^{39}\text{Ar}$  results for alkali feldspars  
325 containing diffusion domains with differing activation energy. *Geochim. Cosmochim. Acta*  
326 55(5), 1435-1448.

327 Harrison, T.M., Grove, M., Lovera, O.M., Zeitler, P.K., 2005. Continuous Thermal Histories  
328 from Inversion of Closure Profiles. *Rev. in Mineralogy and Geochemistry* 58(1), 389-409.

329 Hinze, W.J., Allen, D.J., Braile, L.W., Mariano, J., 1997. The Midcontinent rift system: A major  
330 Proterozoic continental rift. *Geol. Soc. Am. Spec. Paper* 312, 7-35.

331 Holland, T., Blundy, J. 1994. Non-ideal interactions in calcic amphiboles and their bearing on  
332 amphibole-plagioclase thermometry: *Contrib. Mineral. Petrol.* 116, 433-447.

333 Holm, D.K, Lux, D., 1998. Depth of emplacement and tilting of the Middle Proterozoic (1470  
334 Ma) Wolf River batholith, Wisconsin: Ar-Ar thermochronologic constraints. *Can. J. Earth*  
335 *Sci.* 35, 1143-1151.

336 Holm, D., Darrah, K., Lux, D., 1998a. Evidence for widespread ~1760 Ma metamorphism and  
337 rapid crustal stabilization of the Early Proterozoic Penokean orogen, Minnesota. *Am. J. Sci.*  
338 298, 60-81.

339 Holm, D., Schneider, D.A., Coath, C., 1998b. Age and deformation of Early Proterozoic  
340 quartzites in the southern Lake Superior region: Implications for extent of foreland  
341 deformation during final assembly of Laurentia. *Geology* 26, 907-910.

342 Holm D. K., Van Schmus, W. R., Mac Neil, L. C., Boerboom, T. J., Schweitzer, D., Schneider,  
343 D.A., 2005. U-Pb zircon geochronology of Paleoproterozoic plutons from the northern mid-  
344 continent, U.S.A.: Evidence for subduction flip and continued convergence after geon 18  
345 Penokean orogenesis. *Geol. Soc. Am. Bull.* 117, 259-275.

346 Holm, D.K., Schneider, D.A., Rose, S., Mancuso, C., McKenzie, M., Foland, K., Hodges, K.V.,  
347 2007. Proterozoic metamorphism and cooling ages from the southern Lake Superior region,  
348 USA: *Precambrian Res.* 157, 106-126.

349 Hoppe, W., Montgomery, C., Van Schmus, W., 1983. Age and significance of Precambrian  
350 basement samples from northern Illinois and adjacent states: *Journal of Geophysical*  
351 *Research: Solid Earth* 88(B9), 7276-7286.

352 Karlstrom, K.E., Bowring, S., 1993. Proterozoic orogenic history of Arizona, in Van Schmus, W.  
353 R., Bickford, M. E., 23 others, *Transcontinental Proterozoic provinces*, in Reed, J. C., Jr.,  
354 and 6 others, eds., *Precambrian: Conterminous U.S.*: Boulder, Colorado, Geological Society  
355 of America, *The Geology of North America*, C-2, 188-211

356 Karlstrom, K.E., Åhäll, K-I, Harlan, S.S., Williams, M.L., McLelland, J., Geissman, J.W., 2001.  
357 Long-lived (1.8–1.0 Ga) convergent orogen in southern Laurentia, its extensions to Australia  
358 and Baltica, and implications for refining Rodinia. *Precambrian Res.* 111, 5-30.

359 Koppers, A.A.P. 2002. ArArCALC - software for  $^{40}\text{Ar}/^{39}\text{Ar}$  age calculations. *Comp. & Geosci.*  
360 28, 605-619.

361 Larue, D.K., 1983. Early Proterozoic tectonics of the Lake Superior region; tectonostratigraphic  
362 terranes near the purported collision zone. *Geol. Soc. Am. Memoir* 160, 33-47.

363 LaBerge, G.L., Cannon, W.F., Schulz, K.J., Klasner, J.S., Ojakangas, R.W., 2003.  
364 Paleoproterozoic stratigraphy and tectonics along the Niagara suture zone, Michigan and  
365 Wisconsin. In: Cannon, W.F. (Ed.), Part 2 – Field Trip Guidebook, *Inst. Lake Superior*  
366 *Geol.* 49, 1-32.

367 Lovera, O.M., Richter, F.M., Harrison, T.M., 1989. The  $^{40}\text{Ar}/^{39}\text{Ar}$  Thermochronometry for  
368 Slowly Cooled Samples Having a Distribution of Diffusion Domain Sizes. *J. Geophys. Res.*  
369 94(B12), 17917-17935.

370 Lovera, O.M., Heizler, M.T., Harrison, T.M., 1993. Argon diffusion domains in K-feldspar II:  
371 kinetic properties of MH-10. *Contrib. Min. Petrol.* 113, 381-393.

372 Lovera, O.M., Grove, M., Mark Harrison, T., Mahon, K.I., 1997. Systematic analysis of K-  
373 feldspar  $^{40}\text{Ar}/^{39}\text{Ar}$  step heating results: I. Significance of activation energy determinations.  
374 *Geochim. Cosmochimica Acta*, 61(15). 3171-3192.

375 Lovera, O.M., Grove, M., Harrison, T.M., 2002. Systematic analysis of K-feldspar  $^{40}\text{Ar}/^{39}\text{Ar}$   
376 step heating results II: relevance of laboratory argon diffusion properties to nature.  
377 *Geochim. Cosmochimica Acta*, 66(7): 1237-1255.

378 Ludwig, K.R., 2003. Isoplot/Ex, Version 3: A Geochronological Toolkit for Microsoft Excel.  
379 Geochronology Center Berkeley.

380 Maass, R.S. 1983. Early Proterozoic tectonic style in central Wisconsin. In Early Proterozoic  
381 geology of the Great Lakes region. Edited by L.G. Medaris, Jr. Geol. Soc. Am. Memoir 160,  
382 85-89.

383 Maass, R.S., Medaris, L.G., Jr., Van Schmus, W.R., 1980. Penokeyan deformation in central  
384 Wisconsin. In: Morey, G.B., Hanson, G.N. (Eds.), Selected studies of Archean gneisses and  
385 lower Proterozoic rocks, southern Canadian shield. Geol. Soc. Am. Memoir 160, 85-95.

386 McDannell, K.T., 2017. Methods and application of deep-time thermochronology: Insights from  
387 slowly cooled terranes of Mongolia and the North American craton. Theses and  
388 Dissertations. 2721, Lehigh University, Bethlehem, Pennsylvania, 261 p.

389 McDannell, K.T., Zeitler, P.K., Schneider, D.A., 2018. Instability of the southern Canadian  
390 Shield during the late Proterozoic. Earth and Planetary Science Letters, 490: 100-109.

391 McDougall, I., Harrison, T.M., 1999. Geochronology and Thermochronology by the  $^{40}\text{Ar}/^{39}\text{Ar}$   
392 Method, second ed. Oxford University Press, New York, p. 261.

393 McDougall, I., Wellman, P., 2011. Calibration of GA1550 biotite standard for K/Ar and  
394  $^{40}\text{Ar}/^{39}\text{Ar}$  dating. Chem. Geol., 280, 19-25.

395 Medaris, G., Singer, B.S., Dott, R.H., Jr., Naymark, A., Johnson, C.M., Schott, R.C., 2003. Late  
396 Paleoproterozoic climate, tectonics and metamorphism in the southern Lake Superior region  
397 and Proto-North America: Evidence from Baraboo Interval quartzites. J. Geology 111, 243-  
398 257.

399 Medaris, L.G. Jr., Schwartz, J.J., Singer, Bradley S., Jicha, B.R., 2018. Baraboo Interval  
400 quartzites: the Dott legacy and new revelations. Geological Society of America, Programs  
401 with Abstracts, 19-6.

402 Medaris, L.G. Jr., Malone, D.H., Hill, G.C., Singer, Bradley S., Jicha, B.R., Van Lankvelt, A.,  
403 Williams, M.L., Reiners, P.W., 2019. The Wolf River Orogeny: Geon 14 Magmatism,  
404 Sedimentation, and Deformation in the Southern Lake Superior Region: Institute on Lake  
405 Superior Abstracts, 65, 45-46.

406 Murphy, J. Brendan, 2007. Igneous rock associations 8. Arc magmatism II: geochemical and  
407 isotopic characteristics: Geoscience Canada, 34, 7–35.

408 Myers, P.E., Cummings, M.L., Wurdinger, S.R., 1980. Precambrian geology of the Chippewa  
409 valley, Wisconsin. 26<sup>th</sup> Ann. Inst. Lake Superior Geol., Guidebook, Field Trip 1, 35-123.

410 NICE Working Group, 2007. Reinterpretation of Paleoproterozoic accretionary boundaries of the  
411 north-central United States based on a new aeromagnetic-geologic compilation. Precambrian  
412 Res. 157, 71-79.

413 Ola, O., Frederiksen, A., Bollmann, T., van der Lee, S., Darbyshire, F., Wolin, E., Revenaugh, J.,  
414 Stein, C., Stein, S., Wysession, M., 2016. Anisotropic zonation in the lithosphere of Central  
415 North America: influence of a strong cratonic lithosphere on the Mid-Continent Rift.  
416 Tectonophysics 683, 367-381.

417 Paces, J.B., Miller, J.D., 1993. Precise U–Pb age of Duluth Complex and related mafic  
418 intrusions, northeastern Minnesota: geochronological insights into physical, petrogenetic,

419 paleomagnetic, and tectonomagmatic processes associated with the 1.1 Ga midcontinent rift  
420 system. *J. Geophysical Research* 98, 13997–14013.

421 Parrish, R. R. 1990. U-Pb dating of monazite and its application to geological problems, *Can. J.*  
422 *Earth Sci.* 27(11), 1431–1450.

423 Pietrzak-Renaud, N., and Davis, D., 2014. U-Pb geochronology of baddeleyite from the  
424 Belleview metadiabase: Age and geotectonic implications for the Negaunee Iron Formation,  
425 Michigan, *Precambrian Res.* 250, 1-5.

426 Price, W.L., 1977. A controlled random search procedure for global optimisation. *The Computer*  
427 *Journal*, 20(4): 367-370.

428 Reiners, P.W., Ehlers, T.A., Zeitler, P.K., 2005. Past, present, and future of thermochronology.  
429 In: P.W. Reiners and T.A. Ehlers (Editors), *Low-Temperature Thermochronology:*  
430 *Techniques, Interpretations, and Applications. Reviews in Mineralogy and Geochemistry.*  
431 *Mineralogical Society of America and Geochemical Society, Washington, DC, United*  
432 *States*, pp. 1-18.

433 Renne, P., Swisher, C. Deino, A., Karner, D., Owens, T., DePaolo, D., 1998. Intercalibration of  
434 standards, absolute ages and uncertainties in  $^{40}\text{Ar}/^{39}\text{Ar}$  dating. *Chem. Geol.* 145, 117-152.

435 Romano, D., Holm, D.K., Foland, K., 2000. Determining the extent and nature of Mazatzal-  
436 related overprinting of the Penokean orogenic belt in the southern Lake Superior region,  
437 north-central USA. *Precambrian Res.* 104, 25-46.

438 Schmitt, A., Grove, M., Harrison, T.M., Lovera, O.M., Hulen, J., Waters, M., 2003. The  
439 Geysers–Cobb Mountain Magma System, California (Part 1): U–Pb zircon ages of volcanic  
440 rocks, conditions of zircon crystallization and magma residence times. *Geochim.*  
441 *Cosmochimica Acta* 67, 3423–3442. doi:10.1016/S0016-7037(03) 00140-6.

442 Schneider, D.A., Bickford, M.E., Cannon, W., Shulz, K., Hamilton, M., 2002. Age of volcanic  
443 rocks and syndepositional iron formations, Marquette Range Supergroup: implications for  
444 the tectonic setting of Paleoproterozoic iron formations of the Lake Superior region. *Can. J.*  
445 *Earth Sci.* 39, 999-1012.

446 Schneider, D.A., Holm, D.K., O’Boyle, C., Hamilton, M., Jercinovic, M., 2004. Paleoproterozoic  
447 development of a gneiss dome corridor in the southern Lake Superior region, USA: *In*  
448 Whitney et al. (eds) *Gneiss domes in orogeny*: Geol. Soc. Am. Special Paper 380, 339-357.

449 Schulz, K.J., 1987. An Early Proterozoic ophiolite in the Penokean orogen [Abstract]:  
450 Geological Society of Canada—Mineralogical Association of Canada, Program with  
451 Abstracts, v. 12, p. 87.

452 Schulz, K.J., Cannon, W.F., 2007. The Penokean orogeny in the Lake Superior region.  
453 *Precambrian Res.* 157, 4-25.

454 Schulz, K.J., Cannon, W.F., Woodruff, L.G., 2018. Geochemistry of mafic rocks in Dickinson  
455 County, Michigan: Evidence for ~2.1 Ga Rifting, 64th Institute on Lake Superior Geology  
456 Proceedings, v. 64, Part 1, Program and Abstracts, p. 93-94

457 Schumacher, J.C, 1997. The Estimation of the proportion of ferric iron in the electron-  
458 microprobe analysis of amphiboles, Appendix 2 in Leake B.E. and 21 others, *Nomenclature*

459 of amphiboles: Report of the subcommittee on amphiboles of the International  
460 Mineralogical Association, Commission on new minerals and mineral names: Canadian  
461 Mineralogist 35, 219-249.

462 Schwartz, Joshua J., Stewart, Esther K., Medaris, L. Gordon Jr., 2018. Detrital Zircons in the  
463 Waterloo Quartzite, Wisconsin: Implications for the Ages of Deposition and Folding of  
464 Supermature Quartzites in the Southern Lake Superior Region, 64th Institute on Lake  
465 Superior Geology Proceedings, v. 64, Part 1, 95-96.

466 Sims, P. K., 1993. Petrography and geochemistry of early Proterozoic granitoid rocks in  
467 Wisconsin Magmatic terranes of Penokean Orogen, northern Wisconsin, US Government  
468 Printing Office, v. 1904.

469 Sims, P.K., Van Schmus, R., Schulz, K., Peterman, Z., 1989. Tectono-stratigraphic evolution of  
470 the Early Proterozoic Wisconsin magmatic terranes of the Penokean orogen. Can. J. Earth  
471 Sci. 26, 2145-2158.

472 Sims, P.K., Klasner, J.S., Peterman, Z.E., 1990. The Mountain shear zone, northeastern  
473 Wisconsin, U.S.A. – a ductile deformation zone within the Early Proterozoic Penokean  
474 orogeny. USGS Bulletin 1904-A.

475 Sims, P.K., Schulz, K.J., Peterman, Z.E., 1992. Geology and geochemistry of Early Proterozoic  
476 rocks in the Dunbar area, northeastern Wisconsin: U.S. Geological Survey Professional  
477 Paper 1517, 65 p.

478 Sims, P.K., Schulz, K.J., 1993, Geologic map of Precambrian rocks in parts of Iron Mountain  
479 and Escanaba 30' X 60' quadrangles, northeastern Wisconsin and adjacent Michigan: U.S.  
480 Geological Survey Miscellaneous Investigations Series Map 1-2356, scale 1:100,000

481 Smith, M.E., Singer, B.S., Carroll, A.R., Fournelle, J.H. (2006) High-resolution calibration of  
482 Eocene strata:  $^{40}\text{Ar}/^{39}\text{Ar}$  geochronology of biotite in the Green River Formation. *Geology*  
483 34, 393-396.

484 Stewart, E.D., Stewart, E.K., Walker, Alex, Zambito, J, J., Jr., 2018. Revisiting the  
485 Paleoproterozoic Baraboo interval in southern Wisconsin: evidence for syn-depositional  
486 tectonism along the south-central margin of Laurentia: *Precambrian Res.*, 314, 221–239.

487 Van Schmus, W.R., Hinze, W.J., 1985. The Mid-Continent Rift System, *Annual Rev. Earth*  
488 *Planet. Sci.* 13, 345-383.

489 Van Schmus, W.R., Thurman, M.E., Peterman, Z.E., 1975. Geology and Rb-Sr chronology of  
490 Middle Precambrian rocks in eastern and central Wisconsin. *Geol. Soc. Am. Bull.* 86, 1255-  
491 1265.

492 Van Schmus, W.R., 1980. Chronology of igneous rocks associated with the Penokean orogeny in  
493 WI. *In* Morey and Hanson (eds) *Selected studies of Archean gneisses and lower Proterozoic*  
494 *rocks, southern Canadian Shield. Geol. Soc. Am. Spec. Paper* 182, 159-168.

495 Van Schmus, W.R., Schneider, D.A., Holm, D.K., Dodson, S., Nelson, B.K., 2007. New insights  
496 into the southern margin of the Archean-Proterozoic transition in the north-central U.S.  
497 based on U-Pb, Sm-Nd, and Ar-Ar geochronology. *Precambrian Res.* 157, 80-105.

- 498 Van Wyck, N., 1995. Oxygen and carbon isotopic constraints on the development of eclogites,  
499 Holsnoy, Norway, and major and trace element, common lead, Sm-Nd, and zircon  
500 geochronology constraints on petrogenesis and tectonic setting of pre- and Early Proterozoic  
501 rocks in Wisconsin. Unpublished Ph.D. thesis, University of Wisconsin, 288 pp.
- 502 Willett, S.D., 1997. Inverse modeling of annealing of fission tracks in apatite 1: A controlled  
503 random search method. *Am. J. Science*, 297(10): 939-969.
- 504 Williams, H., Hoffman, P.F., Lewry, J.F., Monger, J.W.H. Rivers, T. 1991. Anatomy of North  
505 America: thematic geologic portrayals of the continent. *Tectonophysics* 187, 117-134.
- 506 Zeitler, P.K., 2004, Arvert 4.1. Inversion of  $^{40}\text{Ar}/^{39}\text{Ar}$  Age Spectra., User's Manual 2004,  
507 updated Nov. 2017 <http://eesarchive.lehigh.edu/EESdocs/geochron/software.html>.